

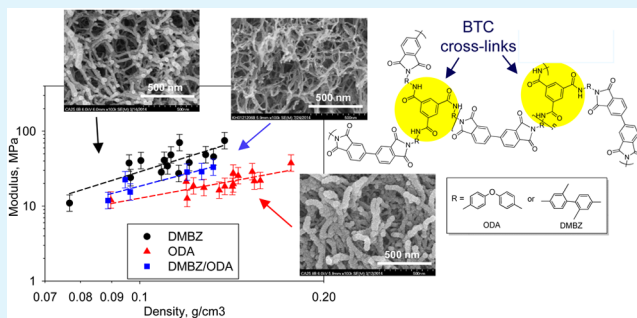
# Polyimide Aerogels with Amide Cross-Links: A Low Cost Alternative for Mechanically Strong Polymer Aerogels

Mary Ann B. Meador,\* Christian R. Alemán,<sup>†</sup> Katrina Hanson,<sup>†</sup> Nakaira Ramirez,<sup>†</sup> Stephanie L. Vivod,  
Nathan Wilmoth,<sup>‡</sup> and Linda McCorkle<sup>§</sup>

NASA Glenn Research Center, 21000 Brookpark Road, Cleveland, Ohio 44135, United States

**ABSTRACT:** Polyimide aerogels combine high porosity, low thermal conductivity, flexibility, and low density with excellent mechanical properties. However, previously used cross-linkers, such as 1,3,5-triaminophenoxybenzene (TAB), 2,4,6-tris(4-aminophenyl)pyridine (TAPP), or octa(aminophenoxy)silsesquioxane (OAPS), either are not commercially available or are prohibitively expensive. Finding more cost efficient cross-linkers that are commercially available to synthesize these aerogels is crucial for making large scale manufacturing attractive. Herein, we describe an approach to making polyimide aerogels starting with amine capped oligomers that are cross-linked with 1,3,5-benzenetricarbonyl trichloride (BTC). BTC is a lower cost, commercially available alternative to TAB, TAPP, or OAPS. Aerogels made in this way have the same or higher modulus and higher surface area compared to those previously reported with either TAB or OAPS cross-links at the same density. While the cross-link structure is an amide, the thermal stability is not compromised most likely because the cross-link is only a small part of the composition of the aerogel. Onset of decomposition depends primarily on the backbone chemistry with 4,4'-oxidianiline (ODA) being more thermally stable than 2,2'-dimethylbenzidine (DMBZ), similar to those previously reported with other cross-links.

**KEYWORDS:** aerogel, polyimide, polyamide, mesoporous, cross-linked



## INTRODUCTION

Aerogels are low density solids with low thermal conductivity, low dielectric constant, high surface area, and other interesting properties due to their fine pore structure.<sup>1,2</sup> Polyimide aerogels combine low thermal conductivity<sup>3</sup> and low dielectric constant<sup>4</sup> with excellent mechanical properties compared to silica<sup>5</sup> and polymer–silica hybrid aerogels.<sup>6</sup> This combination of properties makes them possibly enabling materials for applications ranging from lightweight substrates for high performance antennas<sup>7</sup> to flexible insulation for space suits<sup>8</sup> or inflatable structures for entry, descent, and landing applications.<sup>9</sup> Previously, polyamines, namely, 1,3,5-triaminophenoxybenzene (TAB),<sup>10</sup> 2,4,6-tris(4-aminophenyl)pyridine (TAPP),<sup>11</sup> octa(aminophenoxy)silsesquioxane (OAPS),<sup>12</sup> or 1,3,5-tris(aminophenyl)benzene (TAPB),<sup>13</sup> have been used to cross-link anhydride end-capped oligomers in the synthesis of the polyimide aerogels. However, these cross-linkers are either not commercially available or somewhat expensive, inhibiting scale up and production of the polyimide aerogels for widespread use. Polyimide aerogels made using no cross-linker tend to shrink more during fabrication and seem to be limited to those derived from pyromellitic dianhydride.<sup>14</sup> An alternative route to cross-linked polyimide aerogels that utilizes dianhydrides reacting with triisocyanates claims a room temperature cure.<sup>15,16</sup> However, thermogravimetric analysis (TGA) of room temperature and 90 °C produced aerogels from that

route<sup>15</sup> had weight loss of 5–7% with an onset of about 200 °C, which is indicative of incomplete imidization. Linear polyamide–polyimide clay aerogel composites have also been fabricated and utilize freeze-drying instead of supercritical fluid extraction to remove the liquid.<sup>17</sup> The clay acts as a template for the formation of the porous structure. However, the mechanical properties are lower and the thermal conductivities are higher than polyimide aerogels produced from cross-linked polyimide gels dried by supercritical fluid extraction.<sup>18</sup>

Herein, we present a new synthesis for polyimide aerogels using a cost-effective, commercially available cross-linker, 1,3,5-benzenetricarbonyl trichloride (BTC), as shown in Scheme 1. BTC has recently been used to cross-link amine terminated polyamide oligomers to fabricate polyamide aerogels.<sup>19</sup> Similar to that approach, instead of synthesizing anhydride terminated oligomers to cross-link with polyamines, we generate amine capped polyimide oligomers in solution that are first chemically imidized. Then the triacid chloride is added to the solution to produce gels with triamide cross-links.

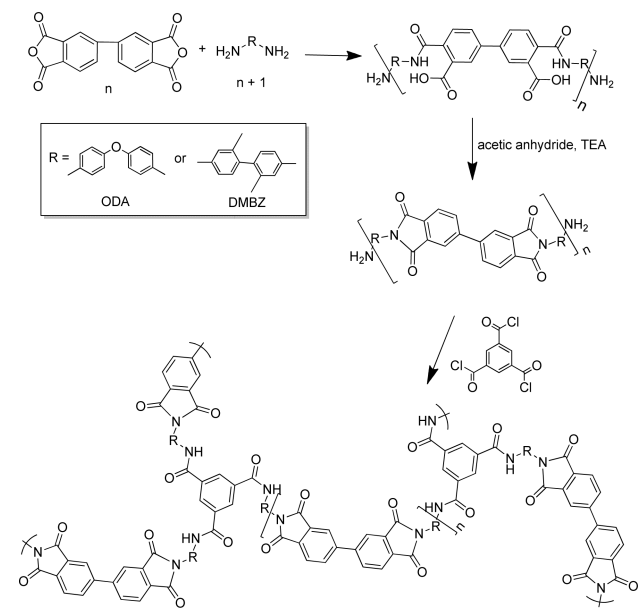
In this study, we also use backbone chemistry similar to that previously reported for polyimide aerogels made with TAB and OAPS so that the properties of the triamide cross-linked

Received: October 20, 2014

Accepted: December 19, 2014

Published: January 7, 2015

**Scheme 1. Synthesis of Polyimide Aerogels Cross-Linked Using BTC**



structures can be easily compared to the previous work. In this regard, we utilize biphenyl-3,3',4,4'-tetracarboxylic dianhydride (BPDA) as shown in Scheme 1 and either 2,2'-dimethylbenzidine (DMBZ), 4,4'-oxidianiline (ODA), or a 50/50 combination of the two as diamine to synthesize the polyimide oligomers. The aerogels in the study are characterized by NMR, FTIR, helium pycnometry, nitrogen sorption, scanning electron microscopy, compression testing, and thermal analysis. Repeat units in the oligomers,  $n$ , are varied between 10 and 40 by using a ratio of  $n$  dianhydride units to  $(n + 1)$  diamine units to fabricate the oligomers as shown in Scheme 1 to study the effect of cross-link density on the properties of the aerogels. In addition, the concentration of total polymer in the gelation solution is varied from 7 to 10 wt % in order to assess the effect of changing the density on the properties.

## EXPERIMENTAL SECTION

**Materials.** Acetic anhydride (AA), triethylamine (TEA), and 1,3,5-benzenetricarbonyl trichloride (BTC) were purchased from Sigma-Aldrich (3050 Spruce Street, St. Louis, MO 63103). Anhydrous *N*-methylpyrrolidinone (NMP) was purchased from Tedia (1000 Tedia Way, Fairfield, OH 45014). 2,2'-Dimethylbenzidine (DMBZ), 4,4'-oxidianiline (ODA), and biphenyl-3,3',4,4'-tetracarboxylic dianhydride (BPDA) were obtained from Chriskey, Inc. (13920 W. 108th Street, Lenexa, KS 66215). Dianhydrides were dried at 125 °C in vacuum for 24 h before use. All other reagents were used without further purification.

**General.** Nitrogen-adsorption porosimetry was carried out with an ASAP 2000 surface area/pore distribution analyzer (Micrometrics Instrument Corp.). A Micrometrics Accupyc 1340 helium pycnometer was used to measure the skeletal density of the specimens. A TA model 2950 HiRes instrument was used to perform thermal gravimetric analysis (TGA). Thermomechanical analysis was performed using a TMA 2940 from TA Instruments. Infrared spectroscopy was performed using a Nicolet Nexus 470 FTIR spectrometer. A Bruker Avance 300 spectrometer was used to obtain  $^{13}\text{C}$  NMR spectra of the polymers. Scanning electron microscopy (SEM) was performed using a Hitachi S-4700 field emission microscope after sputter-coating the specimens with platinum. Mechanical compression testing was performed following ASTM D695-10 standard as previously described.<sup>4</sup>

Experimental design and analysis were conducted using Design Expert, version 8.1, available from Stat-Ease, Inc. (Minneapolis, MN, USA). An experimental design with three variables, including diamine (ODA or DMBZ), total polymer concentration (7–10 wt %), and number of repeat units  $n$  (10–40) in the amine terminated oligomers, was carried out. A total of 36 separate batches of aerogel were produced in the study as shown in Table 1, including eight repeats scattered randomly throughout the design to assess model reliability and accuracy. Data from the experiments were analyzed using multiple linear regression. A full quadratic equation of the variables, including all two-way interactions, was entertained for each response, and backward stepwise regression was carried out to eliminate terms deemed not significant from the model.

**Preparation of BTC Cross-Linked Polyimide Monoliths.** The aerogels were fabricated as shown in Scheme 1, starting with synthesis of amine end-capped polyimide oligomers with  $n$  repeat units using  $n$  equiv of BPDA and  $n + 1$  equiv of diamine. The oligomers were cross-linked with BTC to form gels. Concentration of total polymer in the gelation solution (7–10 wt %), type of diamine used (DMBZ or ODA), and number of repeat units in the oligomers ( $n = 10$ –40) were varied in the fabrication of the aerogels as shown in Table 1. As an example, the procedure for formulation 9 from Table 1 using DMBZ,  $n = 40$ , and polymer concentration of 7 wt % is carried out as follows: To a solution of DMBZ (3.18 g, 15 mmol) in 80 mL of NMP was added BPDA (4.31 g, 14.6 mmol), and the solution was stirred until fully dissolved. Afterward, acetic anhydride (11.07 mL) was added and stirred until homogeneously mixed, followed by TEA (2.04 mL). After about 15 min, a solution of BTC (0.065 g, 0.24 mmol) in 10 mL of NMP was added to this solution while stirring. Immediately after mixing, the solution was poured into the molds. The solutions gelled after about 10–15 min. The gels were aged for 24 h in the mold and then were extracted into a solution of 75% NMP in acetone and soaked overnight. Afterward, the solvent was replaced by a solution of 25% NMP in acetone and the gels were soaked for another 24 h, followed by three more solvent exchanges in 100% acetone in 24 h intervals. The gels were then converted to aerogels by supercritical fluid extraction. This was accomplished in multiple steps that included subcritical and supercritical CO<sub>2</sub> soaking and rinsing. The gels were submerged in acetone in a sealed chamber at 78 bar and 25 °C. The chamber was then set in a soak mode for 30 min followed by a subcritical liquid CO<sub>2</sub> flush equal to the volume of the chamber and repeated four times. Then the temperature in the chamber was ramped to 35 °C to reach a supercritical state of CO<sub>2</sub> and held for 30 min followed by slow venting (10 g/min) for approximately 2 h. This process was then followed by vacuum drying overnight at 75 °C to remove any residual acetone. The resulting aerogels had a density of 0.100 g/cm<sup>3</sup> and porosity of 92.6%. Solid  $^{13}\text{C}$  NMR (ppm): 165.3, 136.2, 130.6, 123.4, 18.9. FTIR ( $\delta$ ): 1775.8, 1717.5, 1612.8, 1490.2, 1361.9, 1090.9.

Note that all of the aerogels in the study were made as described by first dissolving all of the diamine and adding dianhydride, with the exception of those made from 10 wt % solution and a 50/50 combination of ODA and DMBZ as diamine. These were made by dissolving ODA in solution first, followed by all of the dianhydride. After the dianhydride was completely dissolved, DMBZ was added. This forces the oligomer to have a backbone structure where the diamines are alternating instead of random. The reason for this is outlined in the section Results and Discussion.

## RESULTS AND DISCUSSION

Polyimide aerogels using BTC as the cross-linker were fabricated according to Scheme 1. The variables used to fabricate the aerogels are shown in Table 1, along with density, porosity, surface area, compression properties, and thermal data for each run. The aerogels produced in the study were yellow in appearance, similar to polyimide aerogels using either OAPS or TAB as the cross-linker. However, the BTC gels do seem to form faster than those made using OAPS or TAB. Certain

**Table 1.** Properties of the Different Polyamide Aerogels Investigated in This Study

sample	<i>n</i>	diamine	polymer concn, wt %	density, g/cm <sup>3</sup>	porosity, %	surface area, m <sup>2</sup> /g	modulus, MPa	stress at 10% strain (MPa)	onset of decomposition, °C
1	30	DMBZ	10.0	0.132	90.2	513	45.4	1.5	510.2
2	10	DMBZ	10.0	0.108	92.0	526	<i>a</i>	<i>a</i>	500.0
3	30	ODA	10.0	0.153	90.0	405	28.8	0.87	598.7
4	10	ODA	10.0	0.123	91.3	440	18.6	<i>a</i>	602.5
5	30	DMBZ	7.0	0.097	92.9	550	24.0	0.67	510.9
6	10	DMBZ	7.0	0.077	94.3	539	11.0	0.36	526.3
7	30	ODA	7.0	0.120	92.1	418	12.6	0.48	594.0
8	10	ODA	7.0	0.090	94.1	466	12.0	<i>a</i>	592.2
9	40	DMBZ	7.0	0.100	92.6	555	40.5	0.76	514.6
10	40	ODA	7.0	0.138	90.5	382	18.3	0.64	591.9
11	40	DMBZ	10.0	0.138	89.8	542	74.8	1.65	515.9
12	30	ODA	8.5	0.142	91.3	409	27.6	0.69	598.1
13	30	ODA	8.5	0.142	89.8	406	19.7	0.64	587.3
14	30	DMBZ	8.5	0.110	91.5	560	40.9	0.97	514.6
15	30	ODA	8.5	0.135	89.8	409	16.3	0.61	584.1
16	30	DMBZ	8.5	0.112	92.1	578	48.3	1.05	516.7
17	20	DMBZ	10.0	0.128	89.9	546	48.5	1.35	511.1
18	30	DMBZ	8.5	0.116	91.8	531	27.2	1.11	513.3
19	20	DMBZ	8.5	0.108	91.5	556	28.4	0.92	507.9
20	30	ODA	8.5	0.142	89.5	395	18.3	0.66	580.0
21	20	DMBZ	7.0	0.096	92.4	571	37.6	0.65	515.6
22	40	ODA	8.5	0.157	88.4	444	22.0	0.81	583.9
23	20	ODA	10.0	0.154	88.8	388	21.6	0.82	588.1
24	30	DMBZ	8.5	0.116	91.5	558	70.4	1.10	510.3
25	20	ODA	7.0	0.119	91.6	423	21.3	0.45	591.6
26	40	ODA	10.0	0.177	87.4	374	37.6	1.08	589.1
27	20	ODA	8.5	0.127	90.5	397	17.6	0.56	599.4
28	30	DMBZ	8.5	0.111	91.6	548	34.3	1.04	515.5
29	30	ODA	8.5	0.145	89.6	379	25.5	0.74	586.5
30	40	DMBZ	8.5	0.120	90.8	488	38.0	1.16	520.9
31	20	DMBZ/ODA	7.0	0.085	94.4	504	11.9	0.39	531.52
32	30	DMBZ/ODA	7.0	0.092	93.5	476	15.4	0.47	<i>a</i>
33	40	DMBZ/ODA	7.0	0.091	93.9	477	22.5	0.44	535.86
34	20	DMBZ/ODA	10.0	0.120	88.1	493	28.5	0.77	544.73
35	30	DMBZ/ODA	10.0	0.126	89.1	474	28.9	0.89	539.01
36	40	DMBZ/ODA	10.0	0.132	87.3	437	33.1	0.97	540.41

<sup>a</sup>Not measured.

formulations of OAPS or TAB can take up to an hour to gel, whereas the BTC gels form in 5–20 min. This could be due to the fact that the anhydride end-caps on the oligomers compete with acetic anhydride in the reaction with the amines on TAB or OAPS, though acyl groups are not evident in NMR spectra of TAB<sup>10</sup> or OAPS<sup>12</sup> aerogels. Faster gelation of BTC aerogels may also be due to the acid chloride being more reactive toward amine than the anhydride end-caps are in the OAPS or TAB aerogels.

Figure 1 shows solid NMR spectra of selected formulations from the study. Spectra of all aerogel formulations, as expected, have peaks for imide carbonyl (165.3 ppm) and aromatic carbons (120–145 ppm). ODA derived polyimide aerogels (Figure 1a,b) also have a peak at 153.2 ppm (oxygen substituted aromatic carbon) and a small peak at 23 ppm which may indicate a small amount of acylation of the amine end-caps due to a side reaction with acetic anhydride. DMBZ aerogels (Figure 1c,d) have a methyl peak at 18.9 ppm and no evidence of acylation, possibly because DMBZ is overall less reactive than ODA. FTIR of the aerogels exhibit imide carbonyl peaks (1776, 1717 cm<sup>-1</sup>), and TGA curves (vide infra) show

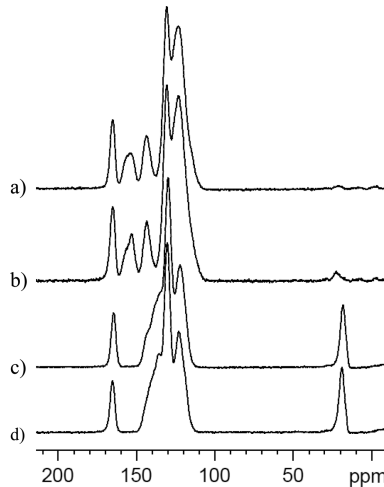


**Figure 1.** <sup>13</sup>C CP-MAS spectra of representative aerogels from the study: (a) ODA (sample 26, 10 wt % *n* = 40); (b) ODA (sample 4, 10 wt %, *n* = 10; (c) DMBZ aerogel (sample 11, 10 wt %, *n* = 40); (d) DMBZ (sample 2, 10 wt %, *n* = 10).

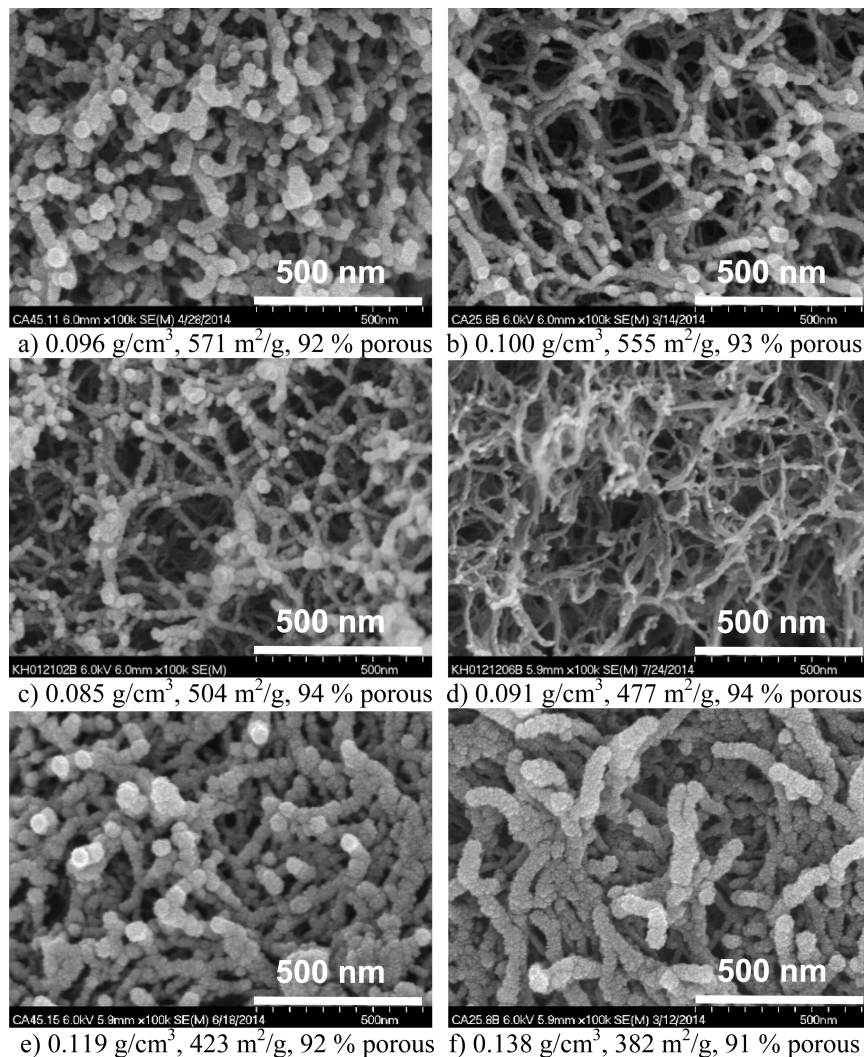


**Figure 2.** Comparison of SEMs of polyimide aerogels made with DMBZ: (a) 7 wt %,  $n = 20$  (sample 21) and (b) 7 wt %  $n = 40$  (sample 9). DMBZ/ODA: (c) 7 wt %,  $n = 20$  (sample 33) and (d) 7 wt %,  $n = 40$  (sample 38). ODA: (e) 7 wt %,  $n = 20$  (sample 25) and (f) 7 wt %,  $n = 40$  (sample 10).

very little weight loss below the onsets of decomposition at 500–600 °C, indicating that imidization at room temperature has gone to completion.

Scanning electron microscopy (SEM) results of representative aerogels in the study made with 7 wt % polymer concentration are shown in Figure 2. Similar to other polyimide aerogels previously reported made with TAB or OAPS cross-linkers, the aerogels have a somewhat fibrous appearance. DMBZ containing formulations (Figure 2a and Figure 2b) and those derived from 50% DMBZ and 50% ODA (Figure 2c and Figure 2d) had finer strands than those derived from ODA alone (Figure 2e and Figure 2f). Samples made from 10 wt % polymer concentration and either ODA or DMBZ alone had morphologies very similar to those shown at 7 wt %. However, as seen in Figure 3, aerogels made using 50% DMBZ and 50% ODA at 10 wt % looked very different. Figure 3a and Figure 3b show SEM results of DMBZ/ODA aerogel made with  $n = 20$  and 10 wt %. These display a more coarse structure that at lower magnification shows that the polymer strands have organized into spheres. This is similar to the morphology seen with previously reported polyimide aerogels containing a mixture of fluorinated and nonfluorinated monomers<sup>4</sup> which was attributed to macroscale phase separation during gelation.

Here, the phenomenon is only seen when concentration of polymer is high, leading one to believe that it is related to how fast gelation occurs. Lowest  $n$  and highest concentration lead to the fastest gel times. Slower gelation may allow the polymer chains to equilibrate. This type of hierarchical porosity has not been observed in OAPS cross-linked aerogels made using 10 wt % polymer and 50% DMBZ/50% ODA which also tend to gel slower.<sup>12</sup> In any case, this issue was solved by making the 10 wt % DMBZ/ODA aerogels in a way that forces an alternating structure in the oligomer backbone. This was achieved by dissolving first one diamine (ODA) in the reaction mixture, followed by all of the dianhydride. Essentially, this creates a solution that mostly consists of  $n = 1$  oligomers of the structure BPDA-ODA-BPDA. Addition of DMBZ should result in an amine capped oligomer backbone with the amines alternating. As shown in Figure 3c and Figure 3d, morphology of these aerogels with an alternating backbone more closely resembles the rest of the aerogels in the study made using either ODA or DMBZ. Thus, this technique prevents the macroscale phase separation from occurring during gelation. Since the difference in morphology can affect other aerogel properties, the data given for the DMBZ/ODA aerogels in Table 1 are all from the

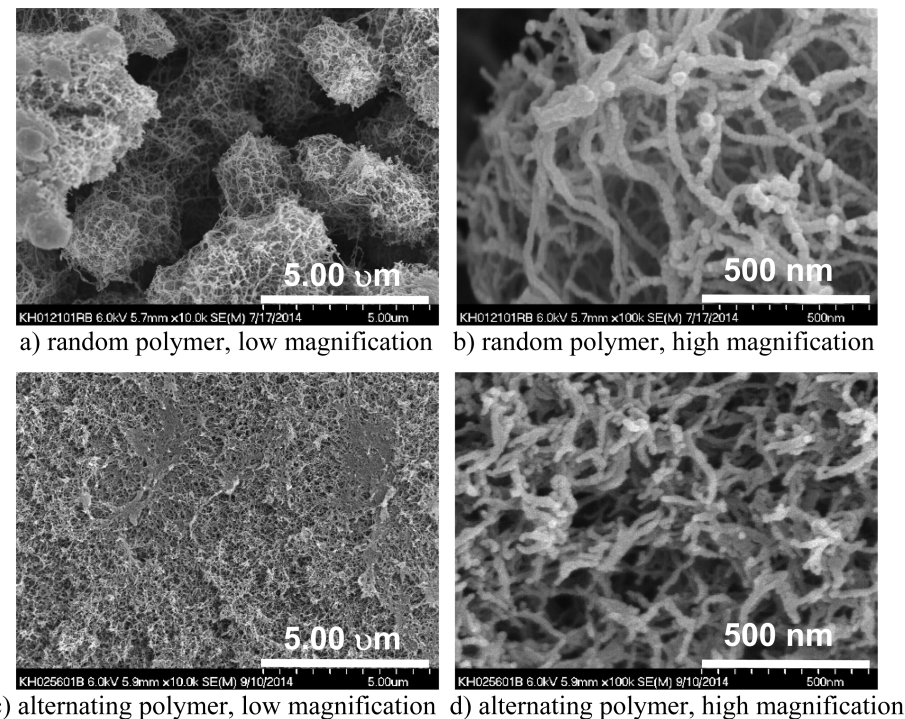


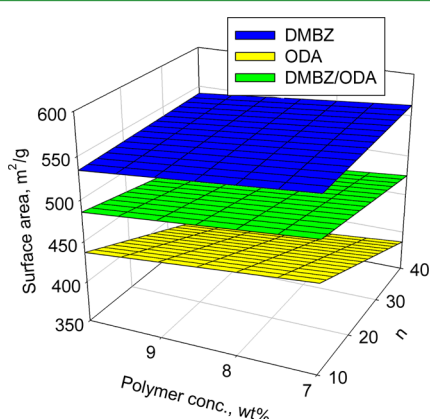
**Figure 3.** SEM results of polyimide aerogels made with DMBZ/ODA and 10 wt % polymer and  $n = 20$  (sample 34) where diamines are reacted randomly at (a) low magnification and (b) high magnification and where diamines are forced to react in alternating fashion at (c) low magnification and (d) high magnification.

alternating structures. In addition, only the alternating structures are used to generate empirical models.

Surface areas of the BTC cross-linked aerogels were measured using nitrogen sorption analyzed by the Brunauer–Emmett–Teller (BET) method.<sup>20</sup> The empirical model for surface area (standard deviation = 14.6,  $R^2 = 0.96$ ) graphed vs polymer concentration and  $n$  is shown in Figure 4. Highest

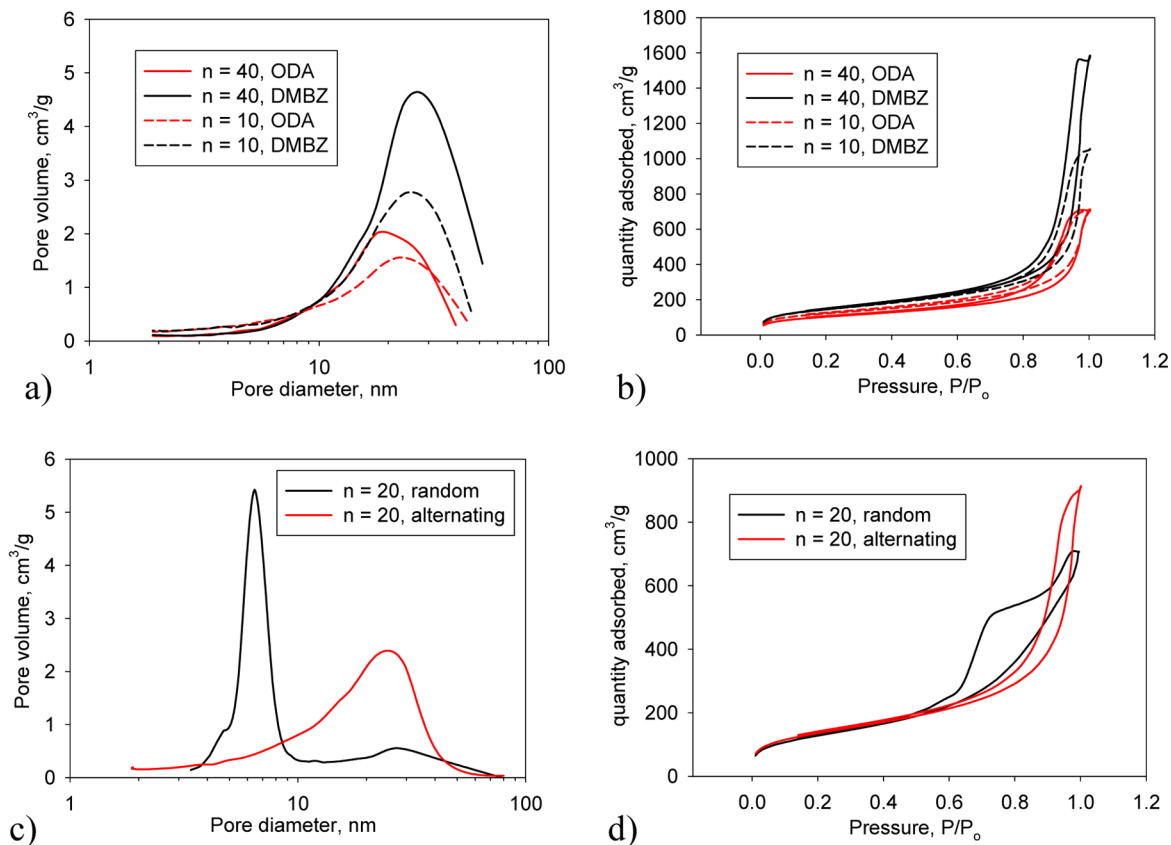
reported with ODA/BPDA in the backbone produced from 10 wt % solutions, surface areas ranged from 202 to 412 m<sup>2</sup>/g. Similar OAPS cross-linked aerogels with ODA/BPDA had surface areas ranging from 254 to 366 m<sup>2</sup>/g, while in this study, surface areas from the same conditions ranged from 375 to 440 m<sup>2</sup>/g depending on  $n$ . Similar increases in surface area are seen for DMBZ/BPDA aerogels in this study (515–546 m<sup>2</sup>/g) compared to the TAB cross-link aerogels previously reported (314–472 m<sup>2</sup>/g). Note that even higher surface areas were obtained at lower polymer concentrations in this study, while only polymer concentrations of 10 wt % were used in the previous studies.

Figure 5a shows graphs of pore volume vs pore diameter of polyimide aerogels cross-linked with BTC made with either ODA or DMBZ. As shown in Figure 5a, the pore size distributions are centered around 20–30 nm for both DMBZ and ODA aerogels. The results for aerogels made using 7 wt % polymer concentration and those made using polymer concentration of 10 wt % (shown) look virtually identical. Adsorption isotherms for these aerogels are IUPAC classification type IV isotherms with H1 or H2 hysteresis as shown in Figure 5b. In contrast, the 50% DMBZ/50% ODA aerogels made with 10 wt % concentrations backbone are shown in Figure 5c. In this graph, it is seen that those made using the alternating backbone are similar to the ones made with ODA or DMBZ alone with the bulk of the pores centered around 20–40 nm. However, interestingly, DMBZ/ODA aerogels with a random backbone have a sharper pore size distribution centered at 6–7 nm and a much smaller, broad peak centered around 30 nm. This indicates that the hierarchical pore structures seen in Figure 3 give rise to a much finer pore structure inside the larger framework. The bimodal pore size distribution is also exhibited by the shape of the adsorption isotherms given in Figure 5d. Here the adsorption isotherm is



**Figure 4.** Graphs showing the empirical model for surface area vs  $n$  and polymer concentration.

surface areas are measured for DMBZ derived aerogels (>500 m<sup>2</sup>/g) followed by those made from DMBZ/ODA. The lowest surface areas are measured for the ODA derived aerogels and range from 375 to 450 m<sup>2</sup>/g. The ranking is similar to surface areas observed for DMBZ and ODA aerogels with TAB<sup>10</sup> or OAPS<sup>12</sup> cross-links. However, the surface areas of the BTC cross-linked aerogels are in general 50–100 m<sup>2</sup>/g higher in all cases. For example, for TAB cross-linked aerogels previously



**Figure 5.** Graphs showing pore volume vs pore diameter and adsorption isotherms for (a, b) ODA and DMBZ aerogels made using 10 wt % polymer concentration and (c, d) 50% DMBZ/50% ODA aerogels made using 10 wt % polymer concentration.

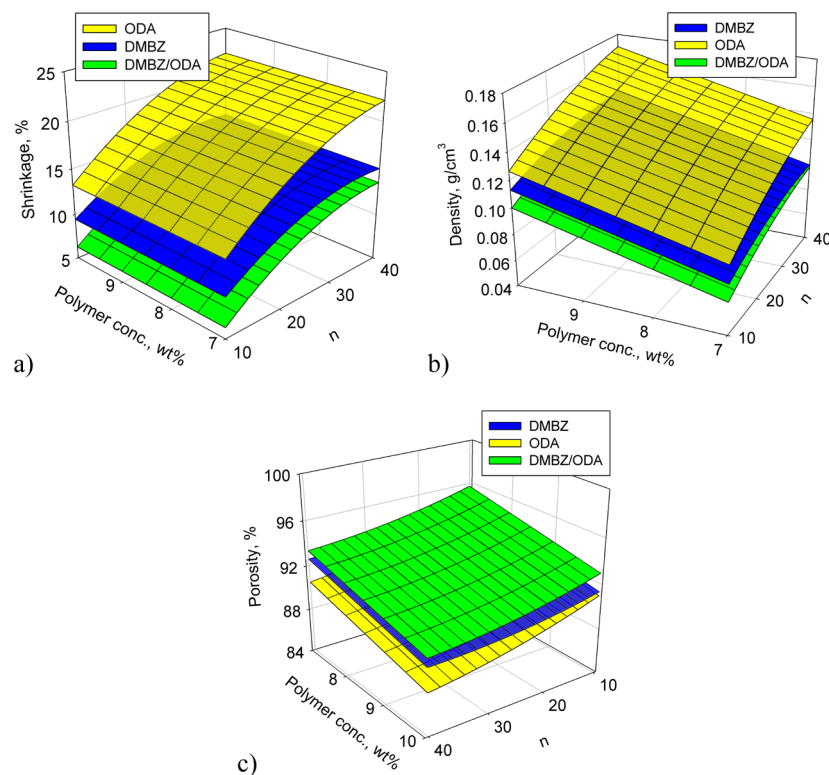


**Figure 6.** Graphs of empirical models for (a) shrinkage, (b) density, and (c) porosity for polyimide aerogels cross-linked with BTC.

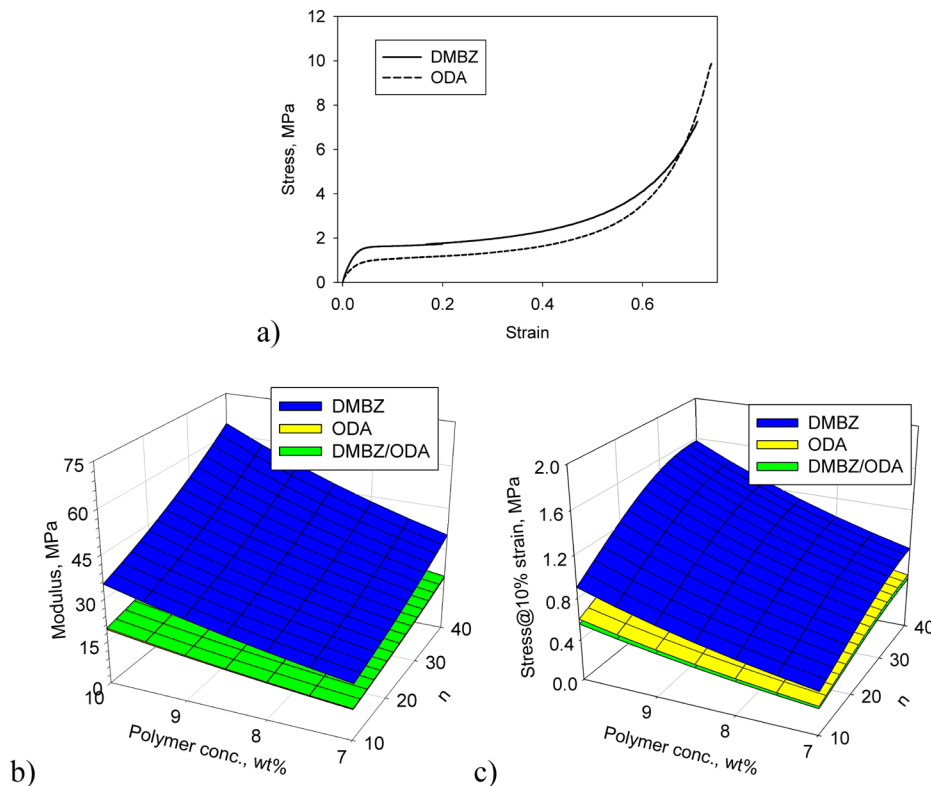


**Figure 7.** Graphs of (a) typical stress–strain curves for compression of the polyimide aerogels (formulations are  $n = 40$  and 10 wt % polymer), (b) the empirical model for modulus vs polymer concentration and  $n$ , and (c) the empirical model for stress at 10% strain vs polymer concentration and  $n$ .

still an IUPAC type IV indicative of mesoporosity but with H3 hysteresis, reflecting the more complex bimodal pore distribution and presence of micropores.<sup>21</sup>

As previously observed for OAPS and TAB cross-linked aerogels, ODA derived aerogels shrink more than DMBZ containing aerogels as measured by comparing the diameter of the aerogels to the diameter of the syringe molds used to form the gels. Some of this shrinkage occurs during formation of the gels, some during solvent exchange, and some during the supercritical drying process. The shrinkage discussed is the total shrinkage occurring during the complete fabrication cycle, as it would be difficult to measure shrinkage of the wet gels. The graph of the empirical model for shrinkage (standard deviation = 1.17%,  $R^2 = 0.93$ ) is shown in Figure 6a. DMBZ/ODA aerogels had the lowest shrinkage. Shrinkage also greatly increases with increasing  $n$  for all backbones. Thus, it follows that the lowest density aerogels as seen in the graph of the empirical model (standard deviation = 0.0046 g/cm<sup>3</sup>,  $R^2 = 0.97$ ) shown in Figure 6b are produced from DMBZ/ODA at the lowest  $n$ . Compared to TAB cross-linked aerogels of the same backbone chemistry, shrinkage and density are slightly lower in this study, while they are similar or slightly lower compared to OAPS cross-linked versions. For example, for TAB cross-linked aerogels previously reported with ODA/BPDA in the backbone produced from 10 wt % solutions, densities ranged from 0.19 to 0.2 g/cm<sup>3</sup>, while in this study, densities from the same conditions ranged from 0.12 to 0.18 g/cm<sup>3</sup> depending on  $n$ . For OAPS cross-linked aerogels previously reported with ODA/BPDA made using 10 wt % polymer concentration, densities ranged from 0.157 to 166 g/cm<sup>3</sup>, within the same range as BTC versions from this study. Similar decreases in density are seen for DMBZ/BPDA aerogels

in this study (0.10–0.12 g/cm<sup>3</sup>) compared to the TAB cross-link aerogels previously reported (0.013–0.15 g/cm<sup>3</sup>) from 10 wt % polymer concentration, while OAPS cross-linked versions with DMBZ (0.086–0.089 g/cm<sup>3</sup>) tended to be lower in density than the BTC aerogels. As seen in Figure 6c, the graph of the empirical model for porosity (standard deviation = 0.58%,  $R^2 = 0.90$ ), as expected, shows the opposite trends from density and shrinkage. The porosity is highest for DMBZ/ODA derived aerogels, and porosity decreases with increasing  $n$  and polymer concentration.

Compression tests were done on all of the aerogels in the study. Typical stress–strain curves are seen in Figure 7a. Young's modulus is taken as the initial slope of the stress strain curve. As shown in the graph of the empirical model for compressive modulus ( $\log(\text{standard deviation}) = 0.11$ ,  $R^2 = 0.76$ ) in Figure 7b, the modulus is highest for DMBZ aerogels and also significantly increases with increasing polymer concentration and increasing  $n$ . The latter is somewhat surprising, since increasing  $n$  results in greater distance between cross-links which might be expected to result in a decrease in modulus. However, since increasing  $n$  results in more shrinkage, it is most likely the higher density that leads to the increase in modulus. Since DMBZ in the backbone results in lower shrinkage and lower density, one might expect lower modulus. However, the modulus is higher because of the greater stiffness of the DMBZ backbone. This is again similar to observations of compressive modulus of OAPS and TAB cross-linked aerogels with the same backbone chemistries. ODA and DMBZ/ODA aerogels show very similar trends in modulus, with the surfaces in the plot in Figure 7b nearly completely overlapping. A graph of the empirical model for compressive strength ( $\log(\text{standard deviation}) = 0.038$ ,  $R^2 = 0.96$ ), taken as the stress at 10% strain,

is shown in Figure 7c. The compressive strength shows the same trends as modulus with the highest strength aerogels being those made from DMBZ at  $n = 40$  and polymer concentration of 10 wt % and the surfaces for ODA and DMBZ/ODA nearly overlapping.

Young's modulus (and compressive strength) typically scales with density in aerogels with similar backbone chemistry. This is true of BTC cross-linked polyimide aerogels as seen in the log-log plot of modulus vs density in Figure 8a. Here it is

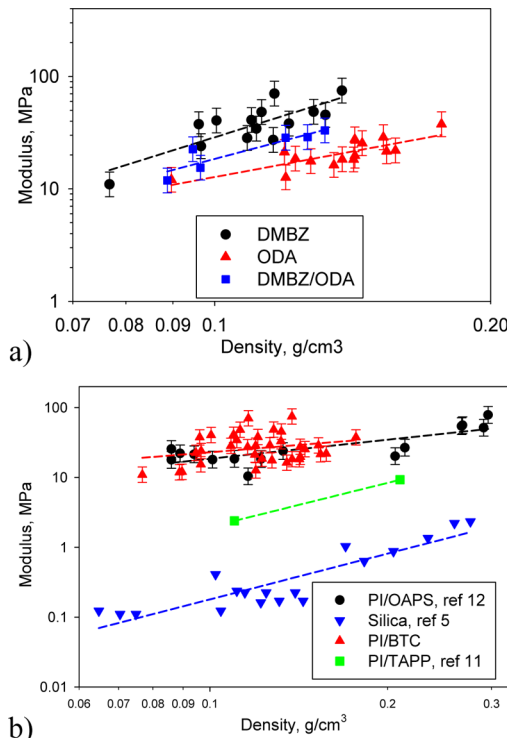


**Figure 8.** Graphs of the relationship of modulus to density (a) comparing ODA (slope = 1.52), DMBZ/ODA (slope = 2.15), and DMBZ (slope = 2.55) polyimide aerogels cross-linked with BTC and (b) comparing BTC cross-linked PI aerogels to other PI aerogels and silica aerogels.

clearly seen that DMBZ derived aerogels at a similar density are the highest in modulus compared to those made with DMBZ/ODA or ODA alone. Figure 8b shows the modulus vs density of all of the BTC cross-linked aerogels from the study

compared with previously reported OAPS<sup>12</sup> and TAPP<sup>11</sup> cross-linked polyimide aerogels and with silica aerogels.<sup>5</sup> As shown in this plot, the BTC cross-linked aerogels are of similar or higher modulus than OAPS cross-linked aerogels at a similar density using the same backbone chemistry. They are also an order of magnitude higher than previously reported PI aerogels cross-linked with TAPP,<sup>11</sup> though these do not have the same oligomer backbone.

It might be expected that using BTC as a cross-link could lower the thermal stability compared to other cross-links because of the resulting amide structure. However, the onsets of decomposition are quite similar to TAB cross-linked aerogels previously reported with the same backbone chemistry,<sup>10</sup> as seen in representative TGA plots of aerogels from the study shown in Figure 9a. As shown in the graph of the empirical model for onset of decomposition (standard deviation = 5.29 °C,  $R^2 = 0.98$ ) in Figure 9b, backbone chemistry has the largest effect on onset of decomposition. As might be expected since the chemistry is not changed, polymer concentration has no effect on onset of decomposition over and above random error. The effect of  $n$  can be interpreted as the effect of cross-linker on onset of decomposition, since BTC concentration goes up with decreasing  $n$ . It is interesting to note that onset of decomposition goes up slightly with increasing  $n$  (decreasing BTC) when DMBZ is the diamine (100% DMBZ) but the opposite is true when ODA is the diamine (0% DMBZ). This suggests that BTC is more thermally stable than DMBZ (pendent methyls) but slightly less thermally stable than ODA (oxygen bridge). Nevertheless, the effect of degradation on the cross-link chemistry is very small.

Onset of decomposition is not the limiting factor in long-term use temperature for the polyimide aerogels. Rather, shrinkage occurs in the aerogels on heating at 150 °C and higher which limits the use temperature. At a given temperature, shrinkage occurs in the first hour or so of aging and then changes little after that as shown in Figure 10a for a sample aerogel formulation heated for 500 h at either 150 or 200 °C. As shown in Figure 10b, density also tends to level off after the initial increase. In all cases, weight loss over the aging time is very small (less than 1%).

Figure 11 shows empirical models for shrinkage and density of the aerogels after 24 h of heating at either 150 or 200 °C. It is seen that the highest shrinkage occurs for aerogels made using 100% DMBZ. After 150 °C aging, total shrinkage of DMBZ aerogels is around 40% (including shrinkage during

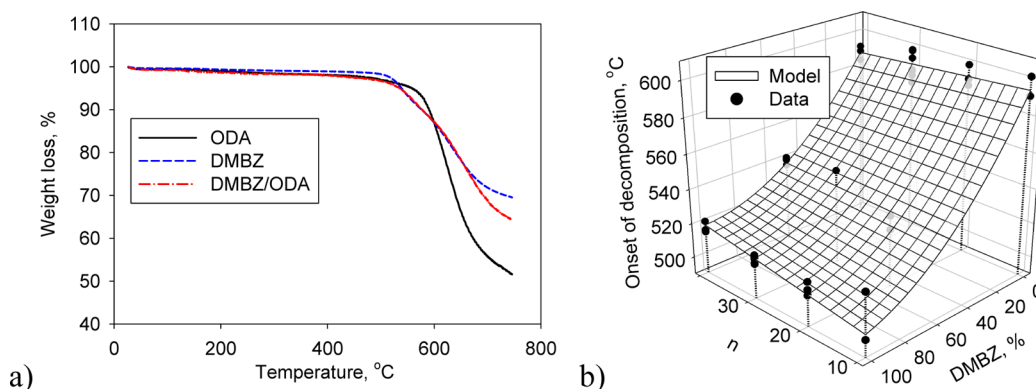


**Figure 9.** Graphs of (a) representative TGA curves from the study and (b) the empirical model for onset of decomposition vs polymer concentration and  $n$ .

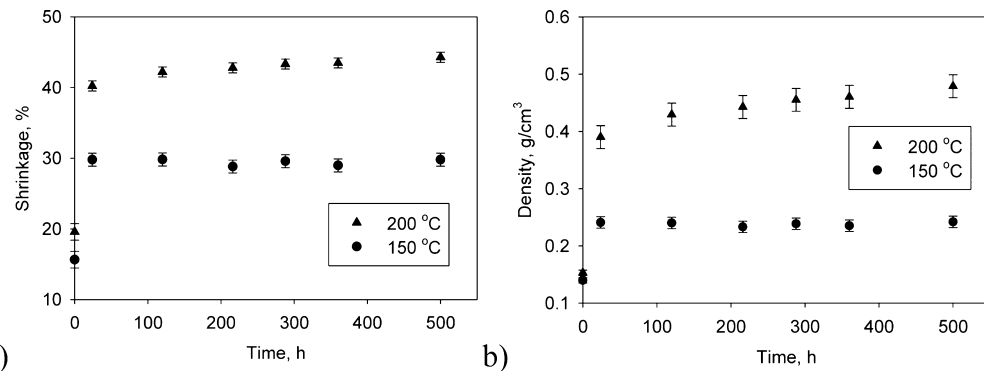


**Figure 10.** Graphs of (a) shrinkage that occurs on heating one aerogel formulation (DMBZ/ODA,  $n = 40$ , 10 wt %) to 150 and 200 °C and (b) resulting density due to shrinkage. Weight loss is negligible.

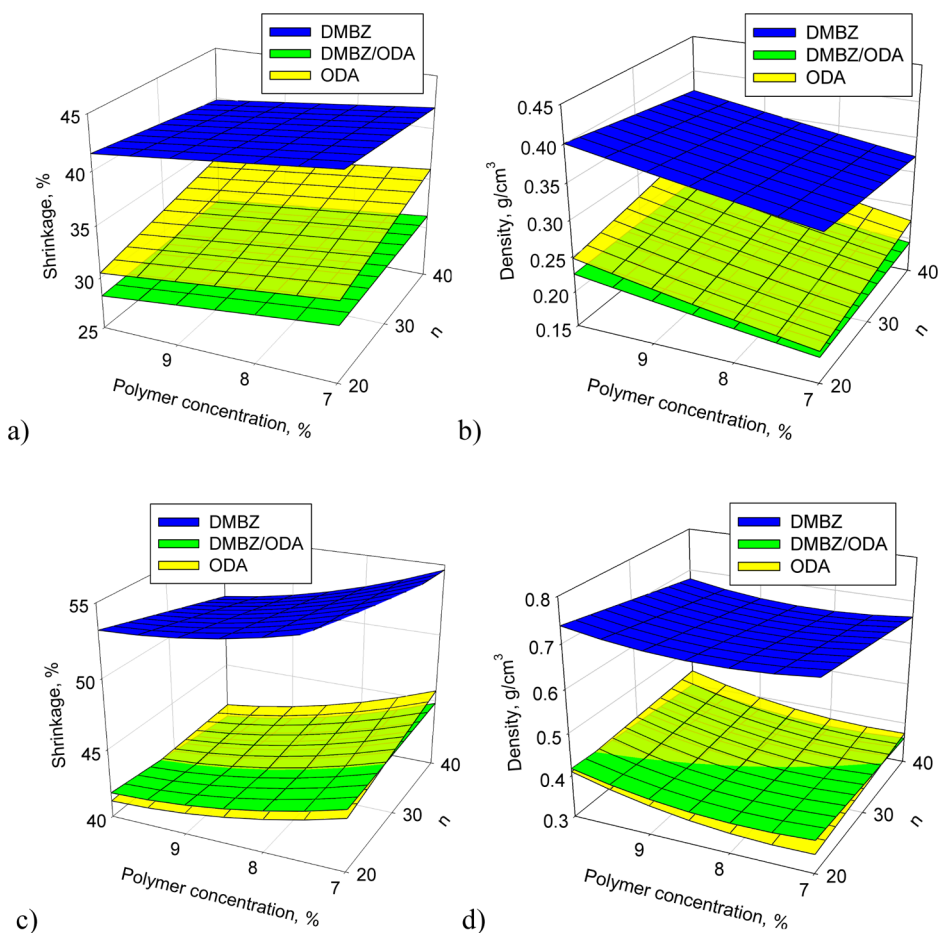


**Figure 11.** Graphs of empirical models for shrinkage that occurs on heating the aerogels to (a) 150 °C and (c) 200 °C and resulting density due to shrinkage at (b) 150 °C and (d) 200 °C.

processing), resulting in aerogels of about 0.38 g/cm<sup>3</sup>. After 200 °C aging, total shrinkage is around 50%, resulting in a density of about 0.64 g/cm<sup>3</sup> after heating. At 150 °C, the lowest shrinkage is seen for aerogels made with 50% DMBZ/50% ODA and  $n = 40$ .

After 150 °C, total shrinkage of these aerogels is around 27%, leading to aerogels of 0.20 g/cm<sup>3</sup>. After 200 °C, aerogels made using ODA or DMBZ/ODA have similar shrinkage and density with total shrinkage around 40–45%, leading to aerogels of 0.35–0.4 g/cm<sup>3</sup>.

## CONCLUSION

Polyimide aerogels with polyamide cross-links were fabricated using amine end-capped polyimide oligomers and BTC as a triacid chloride cross-linker. The use of this alternative and cost-effective cross-linker yields aerogels with the same or better properties than those previously made with more costly or noncommercially available cross-linkers, OAPS, TAPP, and TAB. Modulus from compression was comparable to or better than OAPS cross-linked polyimide aerogels of similar density, while surface areas were significantly higher than the previously reported polyimide aerogels. Since the BTC cross-linker is both

commercially available and less expensive than those previously used, polyimide aerogels derived from BTC may be cost-effective enough to expand from aerospace applications into more terrestrial uses such as insulation for refrigeration, clothing, industrial pipelines, or building and construction. One issue with the BTC cross-linked aerogels is moisture resistance. As previously reported, OAPS cross-linked aerogels containing at least 50% DMBZ were moisture resistant, while the BTC cross-linked aerogels, even those made using 100% DMBZ, absorb water on soaking. Strategies to improve the hydrophobicity of the aerogels are currently being explored.

While the thermal stability might be expected to be lower for the BTC cross-linked polyimide aerogels, onsets of decomposition were very similar and depended more on the backbones of the oligomers. In any case, the use temperature of the aerogels is not limited by the thermal stability of the polymer but rather by shrinkage that occurs on aging at 150 °C and above. Shrinkage occurs on initial heating and levels off, so it is possible to precondition the samples for a particular use temperature. Formulations with a combination of 50% DMBZ/50% ODA shrink the least, resulting in aerogels with density of 0.2 g/cm<sup>3</sup> if preconditioned to 150 °C and aerogels with density of 0.35 g/cm<sup>3</sup> if preconditioned to 200 °C. It may be possible to reduce this shrinkage by the use of other polyimide backbone chemistries or by the addition of nanofillers. These routes are currently being explored.

## AUTHOR INFORMATION

### Corresponding Author

\*maryann.medor@nasa.gov.

### Notes

The authors declare no competing financial interest.

<sup>†</sup>Undergraduate Student Researcher Program (CRA, KH, NR)

<sup>‡</sup>Vantage Partners (NW)

<sup>§</sup>Ohio Aerospace Institute (LM)

## ACKNOWLEDGMENTS

We thank the NASA Game Changing Development Program under the Space Technology Mission Directorate for funding this work. We also thank Dan Scheiman (Ohio Aerospace Institute) for thermal analysis and pycnometry measurements, Baochau Nguyen (Ohio Aerospace Institute) for solid NMR, and Haiquan Guo (Ohio Aerospace Institute) for nitrogen sorption measurements.

## REFERENCES

- (1) Pierre, A. C.; Pajonk, G. M. Chemistry of Aerogels and Their Applications. *Chem. Rev.* **2002**, *102*, 4243–4265.
- (2) Du, A.; Zhou, B.; Zhang, Z.; Shen, J. A Special Material or a New State of Matter: A Review and Reconsideration of the Aerogel. *Materials* **2013**, *6*, 941–968.
- (3) Guo, H.; Meador, M. A. B.; McCorkle, L.; Quade, D.; Guo, J.; Hamilton, B.; Cakmak, M.; Sprowl, G. Polyimide Aerogels Cross-Linked through Amine Functionalized Polyoligomeric Silsesquioxane. *ACS Appl. Mater. Interfaces* **2011**, *3*, 546–552.
- (4) Meador, M. A. B.; McMillon, E.; Sandberg, A.; Barrios, E.; Wilmoth, N. G.; Mueller, C. H.; Miranda, F. A. Dielectric and Other Properties of Polyimide Aerogels Containing Fluorinated Blocks. *ACS Appl. Mater. Interfaces* **2014**, *6*, 6062–6068.
- (5) Fricke, J. Aerogels—Highly Tenous Solids with Fascinating Properties. *J. Non-Cryst. Solids* **1988**, *100*, 169–173.
- (6) Randall, J. P.; Meador, M. A. B.; Jana, S. C. Tailoring Mechanical Properties of Aerogels for Aerospace Applications. *ACS Appl. Mater. Interfaces* **2011**, *3*, 613–626.

(7) Meador, M. A. B.; Wright, S.; Sandberg, A.; Nguyen, B. N.; Van Keuls, F. W.; Mueller, C. H.; Rodríguez-Solís, R.; Miranda, F. A. Low Dielectric Polyimide Aerogels as a Substrate for Lightweight Patch Antennas. *ACS Appl. Mater. Interfaces* **2012**, *4*, 6346–6353.

(8) Paul, H. L.; Diller, K. R. Comparison of Thermal Insulation Performance of Fibrous Materials for the Advanced Space Suit. *J. Biomech. Eng.* **2003**, *125*, 639–47.

(9) Del Corso, J. A.; Cheatwood, F. M.; Bruce W. E.; Hughes, S. J.; Calomino, A. M. Advanced High-Temperature Flexible TPS for Inflatable Aerodynamic Decelerators. Presented at the 21st AIAA Aerodynamic Decelerator Systems Conference, Dublin, Ireland, May 23–26, 2011; 2510.

(10) Meador, M. A. B.; Malow, E. J.; Silva, R.; Wright, S.; Quade, D.; Vivod, S. L.; Guo, H.; Guo, J.; Cakmak, M. Mechanically Strong, Flexible Polyimide Aerogels Cross-Linked with Aromatic Triamine. *ACS Appl. Mater. Interfaces* **2012**, *4*, 536–544.

(11) Shen, D.; Liu, J.; Yang, H.; Yang, S. Highly Thermally Resistant and Flexible Polyimide Aerogels Containing Rigid-Rod Biphenyl, Benzimidazole and Triphenylpyridine Moieties: Synthesis and Characterization. *Chem. Lett.* **2013**, *42*, 1545–1547.

(12) Guo, H.; Meador, M. A. B.; McCorkle, L.; Quade, D. J.; Guo, J.; Hamilton, B.; Cakmak, M. Tailoring Properties of Cross-linked Polyimide Aerogels for Better Moisture Resistance. *ACS Appl. Mater. Interfaces* **2012**, *4*, 5422–5429.

(13) Kawagishi, K.; Saito, H.; Furukawa, H.; Horie, K. Superior Nanoporous Polyimides via Supercritical CO<sub>2</sub> Drying of Jungle Gym Type Polyimide Gels. *Macromol. Rapid Commun.* **2007**, *28*, 96–100.

(14) Rhine, W.; Wang, J.; Begag, R. Polyimide Aerogels, Carbon Aerogels, and Metal Carbide Aerogels and Methods of Making Same. U.S. Patent 7,074,880, 2006.

(15) Chidambareswarapattar, C.; Larimore, Z.; Sotiriou-Leventis, C.; Mang, J. T.; Leventis, N. One-Step Room-Temperature Synthesis of Fibrous Polyimide Aerogels from Anhydrides and Isocyanates and Conversion to Isomorphic Carbons. *J. Mater. Chem.* **2010**, *20*, 9666–9678.

(16) Chidambareswarapattar, C.; Xu, L.; Sotiriou-Leventis, C.; Leventis, N. Robust Monolithic Multiscale Nanoporous Polyimides and Conversion to Isomorphic Carbons. *RSC Adv.* **2013**, *3*, 26459–26469.

(17) Wang, Y.; Al-Biloushi, M.; Schiraldi, D. A. Polymer/Clay Aerogel-Based Glass Fabric Laminates. *J. Appl. Polym. Sci.* **2012**, *124*, 2945–2953.

(18) Guo, H.; Meador, M. A. B.; McCorkle, L.; Quade, D. J.; Guo, J.; Hamilton, B.; Cakmak, M.; Sprowl, G. Polyimide Aerogels Cross-Linked through Amine Functionalized Polyoligomeric Silsesquioxane. *ACS Appl. Mater. Interfaces* **2011**, *3*, 546–552.

(19) Williams, J. C.; Meador, M. A. B.; McCorkle, L.; Mueller, C.; Wilmoth, N. Synthesis and Properties of Step-Growth Polyamide Aerogels Cross-linked with Triacid Chlorides. *Chem. Mater.* **2014**, *26*, 4163–4171.

(20) Brunauer, S.; Emmett, P. H.; Teller, E. Adsorption of Gases in Multimolecular Layers. *J. Am. Chem. Soc.* **1938**, *60*, 309–319.

(21) Sing, K. S. W.; Williams, R. T. Physisorption Hysteresis Loops and the Characterization of Nanoporous Materials. *Adsorpt. Sci. Technol.* **2004**, *22*, 773–782.